Large-conductance Ca^{2+}- and voltage-gated K^+ channels form and break interactions with membrane lipids during each gating cycle

Yutao Tian[a,1], Stefan H. Heinemann[b], and Toshinori Hoshi[a,1]

[a]Department of Physiology, University of Pennsylvania, Philadelphia, PA 19104; and [b]Center for Molecular Biomedicine, Department of Biophysics, Jena University Hospital, Friedrich Schiller University, D-07745 Jena, Germany

Edited by Ramon Latorre, Centro Interdisciplinario de Neurociencias de Valparaíso, Facultad de Ciencias, Universidad de Valparaíso, Valparaíso, Chile, and approved March 19, 2019 (received for review January 24, 2019)

Membrane depolarization and intracellular Ca^{2+} promote activation of the large-conductance Ca^{2+}- and voltage-gated (Slo1) big potassium (BK) channel. We examined the physical interactions that stabilize the closed and open conformations of the ion conduction gate of the human Slo1 channel using electrophysiological and computational approaches. The results show that the closed conformation is stabilized by intersubunit ion–ion interactions involving negative residues (E321 and E324) and positive residues (^{329}RKK^{331}) at the cytoplasmic ends of the transmembrane S6 segments ("RKK ring"). When the channel gate is open, the RKK ring is broken and the positive residues instead make electrostatic interactions with nearby membrane lipid oxygen atoms. E321 and E324 are stabilized by water. When the ^{329}RKK^{331} residues are mutated to hydrophobic amino acids, these residues form even stronger hydrophobic interactions with the lipid tails to promote the open conformation, shifting the voltage dependence of activation to the negative direction by up to 400 mV and stabilizing the selectivity filter region. Thus, the RKK segment forms electrostatic interactions with oxygen atoms from two sources, other amino acid residues (E321/E324), and membrane lipids, depending on the gate status. Each time the channel opens and closes, the aforementioned interactions are formed and broken. This lipid-dependent Slo1 gating may explain how amphipathic signaling molecules and pharmacologically active agents influence the channel activity, and a similar mechanism may be operative in other ion channels.

Slo1 | BK | KCa1.1 | electrophysiology | molecular dynamics

Large-conductance Ca^{2+}- and voltage-gated (Slo1) big potassium (BK) channels function generally as negative-feedback components in cellular electrical excitability by mediating K^+ flux in response to depolarization of transmembrane voltage (V_m) and/or an increase in intracellular Ca^{2+} concentration ($[Ca^{2+}]_i$). Changes in V_m and binding of Ca^{2+} are coupled to opening and closing of the ion conduction gate (1–3). The exact nature of the Slo1 ion conduction gate is yet to be revealed. Subtle changes in the selectivity filter (4–6) and dewetting of the channel cavity (7) have been suggested as the possible underlying mechanisms. Unlike in canonical voltage-gated K^+ channels (8), four Slo1 S6 segments, each capable of rotational movements (9), remain wide apart enough even when the main gate elsewhere is closed, allowing some inhibitors to enter the channel cavity from the intracellular side (4, 10).

Gating of the Slo1 channel is subject to numerous regulatory influences. The channel gene undergoes extensive splicing, producing variants differing at many loci including the area immediately C terminal to S6 (11). Pore-forming Slo1 subunits coassemble with β- and γ-subunits, altering multiple properties such as gating and pharmacology (12). Further, many small molecules, including H_2S, hemin, and various fatty acids and lipids, alter Slo1 gating (13). For example, exogenous intracellular phosphatidylinositol 4,5-bisphosphate (PIP_2), a negatively charged lipid, induces diverse effects (14–16). One main effect of PIP_2 is to increase the open probability (P_o) by ~20-fold without Ca^{2+} at negative voltages where the voltage-sensor activation is negligible (16). This effect of PIP_2 is diminished when the intracellular-facing sequence RKK just C terminal to S6 is mutated to AAA [R329A:K330A:K331A in human Slo1 (hSlo1); AAB65837] (14, 16). Direct interactions of PIP_2 analogs with Lys and Arg are observed in other channels (17, 18), and thus PIP_2 probably binds to the Slo1 RKK segment to increase P_o. The RKK segment is also critical in pharmacological activation of the channel (19).

Here we investigated how the RKK segment of hSlo1 regulates its gating. Our electrophysiological and computational experiments show that the RKK segment interacts with negatively charged residues within the protein when the ion conduction gate is closed but with the membrane phospholipid oxygen atoms when the gate is open. Further, mutation of the RKK segment to hydrophobic amino acids allows the side chains to interact with the lipid tail groups. These gating cycle-by-cycle interactions of the RKK segment with other amino acids and lipids are accompanied by changes in the ion selectivity filter in the structural simulations. The phospholipid-dependent gating of Slo1 may explain how various signaling molecules and pharmacological agents influence the channel activity.

Results

RKK Ring Involving RKK and E321/E324. The sequence ^{329}RKK^{331}, just C terminal to S6, is well conserved in the Slo1 and Slo3 families (*SI Appendix*, Fig. S1). To infer the functional roles of the RKK segment, homology models of hSlo1 were made from the cryo-EM structures of *Aplysia* Slo1 without divalent cations

Significance

Ion channels mediating electrical excitability reside within membrane lipids; however, the nature of the interactions remains obscure. This study shows that specific positive amino acid residues of the Ca^{2+}- and voltage-gated K^+ [big potassium (BK)] channel, a negative-feedback component in cell excitability, form interactions with negative lipid oxygen atoms when the ion conduction gate is open. When the gate is closed, the same positive residues interact with negative residues within the protein. This lipid-dependent gating cycle may explain how cell-signaling molecules and pharmacological modulators of the BK channel work, advancing the fundamental understanding of ion channel function and facilitating therapeutic drug development.

Author contributions: Y.T., S.H.H., and T.H. designed research; Y.T. and T.H. performed research; Y.T., S.H.H., and T.H. analyzed data; and Y.T., S.H.H., and T.H. wrote the paper.

The authors declare no conflict of interest.

This article is a PNAS Direct Submission.

[1]To whom correspondence may be addressed. Email: yttian1983@gmail.com or hoshi@hoshi.org.

This article contains supporting information online at www.pnas.org/lookup/suppl/doi:10.1073/pnas.1901381116/-/DCSupplemental.

Published online April 9, 2019.

(20) and with its divalent cation sensors fully occupied with eight Ca^{2+} and four Mg^{2+} ions (21). Molecular dynamics (MD) simulations of hSlo1 were performed with 150 mM KCl without explicitly simulating a V_m (i.e., 0 mV). The P_o value of hSlo1 without Ca^{2+} at 0 mV is small ($<1 \times 10^{-4}$), while that with divalent cations fully bound is >0.5 (1). Snapshots of the simulated hSlo1 channels are shown in Fig. 1. The RKK segment is situated at the interface between the membrane and intracellular compartment (Fig. 1*A*) in a relatively unstructured area, not well resolved in the divalent cation-free cyro-EM structure (*SI Appendix*, *Materials and Methods*). Viewed from the intracellular side (Fig. 1*B*, *Left*), the RKK segment in the divalent cation-free condition interacts with two negative residues at the C-terminal end of S6 (E321 and E324) in a counterclockwise neighboring subunit (*SI Appendix*, Fig. S2). Thus, the four RKK and E321/E324 segments form a ring of intersubunit ion–ion interactions (hereafter referred to as the RKK ring). E321 and E324 were implicated previously in channel function (22, 23), possibly in conjunction with E219 in S4 (23). We did not observe any obvious interaction between E219 and the RKK segment (*SI Appendix*, Fig. S3).

The RKK ring typically involved the side chains of R329 and K331 interacting with the side-chain O atoms of E321 and less frequently with those of E324 (Fig. 1 *B* and *C*, *Left*). The RKK ring was absent in the divalent cation-bound condition; the RKK residues were positioned away from E321, E324, and the central pore (Fig. 1*B*, *Right* and *SI Appendix*, Fig. S2*B*). The side chains of E321 and E324 in the divalent cation-bound condition were surrounded by water molecules. The existence of the RKK ring exclusively in the divalent cation-free condition suggests that the RKK ring stabilizes a closed conformation and that the lack of the RKK ring is associated with an open conformation of the gate.

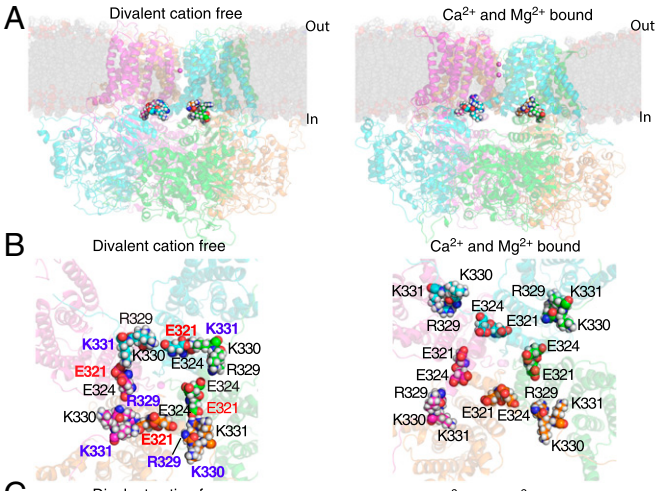

C

Divalent cation free

	R329	K330	K331
E321	**0.426**	0.000	**0.481**
E324	**0.001**	0.000	**0.371**

Ca^{2+} and Mg^{2+} bound

	R329	K330	K331
E321	0.000	0.000	0.000
E324	0.000	0.000	0.000

Fig. 1. Snapshots of simulated hSlo1 without divalent cations and with Ca^{2+} and Mg^{2+}. (*A*) Side view of hSlo1 without divalent cations (*Left*) and with Ca^{2+} and Mg^{2+} (*Right*). Ions outside of the selectivity filter and water are not shown. The channel without divalent cations has only one K^+ in the filter; the outer K^+ ions left the pore earlier in the simulation. (*B*) RKK residues viewed from the intracellular side. The cytoplasmic domain is not shown. ^{329}RKK^{331}, E321, and E324 are shown using spheres. The residues interacting with those with opposite charges are shown in bold. These results are 80 ns after the start of simulation. (*C*) Probability of interactions of ^{329}RKK^{331} with E321 and E324 in hSlo1 without divalent cations (*Left*) and with Ca^{2+} and Mg^{2+} (*Right*) analyzed every 20 ps. The cutoff distance was 3.8 Å. Similar results were obtained in all four simulation runs in each condition.

Mutations of E321 and E324. To validate the simulation results, various RKK ring mutations were electrophysiologically examined. The voltage dependence of channel activation (GV) was described by Boltzmann-type fits to the ionic currents characterized by the half-activation parameter $V_{0.5}$ and the steepness parameter Q_{app}, and these measurements were supplemented with macroscopic kinetics and single-channel measurements to identify which aspects of the gating were altered (13).

If the RKK ring involving ion–ion interactions stabilizes the closed conformation, disruption of the interaction should shift $V_{0.5}$ to the negative direction. Neutralization of E321:E324 to Q (E321Q:E324Q, EE:QQ) and A (E321A:E324A, EE:AA) shifted $V_{0.5}$ without Ca^{2+} by about −100 mV (*SI Appendix*, Table S1) with respect to wild-type (WT) hSlo1 with a mean $V_{0.5}$ of ∼160 mV. The charge-reversal mutant E321R:E324R (EE:RR) showed a similar negative shift (*SI Appendix*, Table S1). The charge-conserving but side-chain-size decreasing mutation E321D:E324D (EE:DD) caused a positive shift of $V_{0.5}$ (*SI Appendix*, Table S1). The negative shifts of $V_{0.5}$ by the charge-neutralization and -reversal mutations are consistent with the idea that the ion–ion interactions of the RKK ring stabilize the closed conformation and keep $V_{0.5}$ positive as observed for WT. The finding that EE:DD caused a positive shift of $V_{0.5}$ suggests that other factors also contribute.

Our simulations point to the greater importance of E321 over E324 (Fig. 1*C*, *Left*). This is consistent with the electrophysiological results from the single mutants E321Q/A and E324Q/A (*SI Appendix*, Table S1). For example, in the double mutant E321Q:E324Q, $\Delta V_{0.5}$ was about −75 mV, while those in the single mutants E321Q and E324Q were about −63 mV and −14 mV, respectively. The $\Delta V_{0.5}$ values for E321Q and E324Q summate roughly to that for the double mutant E321Q:E324Q. Similar results were obtained using E321A, E324A, and E321A:E324A (*SI Appendix*, Table S1). No marked change in Q_{app} was observed with the E321 and E324 mutations (*SI Appendix*, Table S1).

The time course of Slo1 currents at very positive voltages where all four voltage sensors are activated and P_o is near unity reflects the opening kinetics of the ion conduction gate (determined by the rate constant δ_4 in the Horrigan–Aldrich (HA) model) (1, 13, 24), which represents the stability of the closed conformation at such voltages. The activation kinetics of the EE:QQ, EE:AA, and EE:RR mutants at extreme positive voltages were ∼10-fold faster than in WT (Fig. 2), indicative of destabilized closed conformations. The voltage dependence of the activation kinetics was also slightly steeper (Fig. 2). In contrast, the charge-conserving mutant EE:DD showed moderately slower activation kinetics (Fig. 2).

The deactivation kinetics at negative voltages reflect the stability of the open conformation of the ion conduction gate, as specified by the rate constant γ_0 in the HA model (1, 13, 24). The deactivation kinetics of the charge-neutralization and -reversal mutants (EE:QQ, EE:AA, and EE:RR) were ∼10-fold slower in the range of −240 to −200 mV compared with WT (Fig. 2*C*). Thus, the absence of negative residues at positions 321 and 324 leads to greater net stabilization of the open conformation. Without the negative residues, the RKK segment could interact with a different partner to stabilize the open conformation. E321 and E324 may also compete for the interaction with the RKK segment. The voltage dependence of the deactivation kinetics in the mutants was also noticeably shallower (Fig. 2*C*). In the charge-conserving mutant (EE:DD), the deactivation time course was similar to that in WT (Fig. 2*C*).

The closed–open equilibrium of the ion conduction gate was estimated from single-channel measurements at very negative voltages without Ca^{2+}. In WT, the P_o values at –120 mV ($V_{0.5}$ – 280 mV) were = 1.8×10^{-6}. In EE:AA, openings at negative voltages were much more frequently observed and the estimated P_o value at −200 mV ($V_{0.5}$ – 280 mV) was 9.0×10^{-4}, ∼500-fold greater (*SI Appendix*, Fig. S4). The mean open duration for EE:AA was also ∼2.7 longer than for WT at −200 mV (*SI Appendix*,

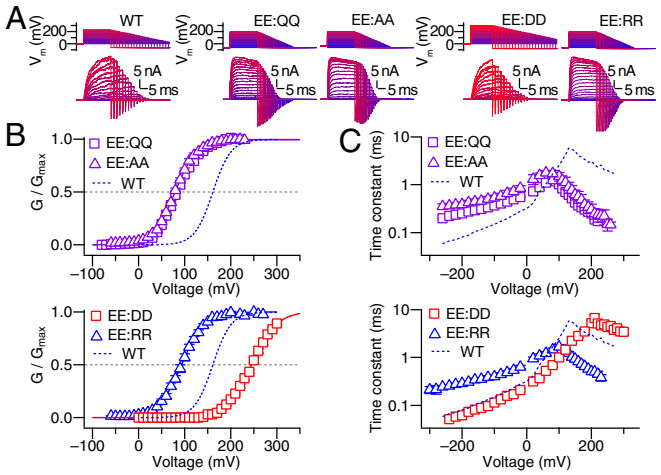

Fig. 2. Double mutations of E321 and E324 in the RKK ring. (*A*) K^+ currents from WT, E321Q:E324Q (EE:QQ), E321A:E324A (EE:AA), E321D:E324D (EE:DD), and E321R:E324R (EE:RR). (*B*) Voltage dependence of steady-state activation. See *SI Appendix*, Table S1 for $V_{0.5}$ and Q_{app}. (*C*) Voltage dependence of current kinetics. The blue dashed curves represent WT. The results shown are means ± SD. Results were obtained with 0 Ca^{2+} with 11 mM EGTA.

Fig. S4). Because gating of Slo1 at extreme negative voltages without Ca^{2+} simplifies to the two-state closed–open model (24), the mean closed duration is estimated to be ∼180 times shorter or that the opening rate constant value [δ_0 in the HA model] is ∼180 greater in EE:AA. Clearly, the closed conformation is destabilized in EE:AA and likely in EE:QQ and EE:RR.

Using the voltage dependence of current kinetics (Fig. 2*C*) and the P_o value at −200 mV, the 0-mV closed–open equilibrium constant L_0 (24) for EE:AA was estimated to be 4.4×10^{-2}, nearly 900-fold greater than that for WT (*SI Appendix*, Table S3). The changes in L_0 and its voltage dependence (z_L) with weakened coupling between the gate and the voltage sensors (D) can account for the observed change in $V_{0.5}$ in EE:AA without Ca^{2+}, $\Delta V_{0.5} = -75$ mV (*SI Appendix*, Fig. S5 and Table S3). The negative shifts in $V_{0.5}$ by the mutations covering E321 and E324 most probably involve alterations of the intrinsic behavior of the ion conduction gate, especially the opening rate constants (δ_{0-4}) reflecting the closed-state stability.

RKK Mutations. The RKK ring stabilizes the closed conformation. To assess whether the RKK segment may also stabilize the open conformation, various mutations of the RKK segment were studied. The charge-conserving mutants R329K (RKK:KKK) and K330R:K331R (RKK:RRR) were virtually identical to WT (Fig. 3, *First Row*; *SI Appendix*, Table S2), illustrating the importance of the positive character of the RKK segment. Neutralization of the RKK segment using polar amino acids, R329Q:K330Q:K331Q (RKK:QQQ) and R329N:K330N:K331N (RKK:NNN), shifted $V_{0.5}$ to the positive direction and decreased Q_{app} (Fig. 3, *Second Row*; *SI Appendix*, Table S2). Like RKK:QQQ and RKK:NNN, the charge-reversal mutations R329E:K330E:K331E (RKK:EEE) and R329D:K330D:K331D (RKK:DDD) shifted $V_{0.5}$ to the positive direction by ∼100 mV and decreased Q_{app} (Fig. 3, *Third Row*; *SI Appendix*, Table S2). The positive shifts in $V_{0.5}$ in the charge-neutralization and -reversal mutants are not expected from the idea that the only role of the RKK segment is to stabilize the closed conformation via ion–ion interactions with E321/E324. The RKK segment must also stabilize the open conformation utilizing its positive charges; this issue will be explored below. The activation kinetics in the RKK:QQQ, RKK:DDD, and RKK:EEE mutants were a few-fold faster at positive voltages (Fig. 3*C*), indicative of the destabilized closed conformations in these mutants but the deactivation kinetics of these mutants at negative voltages were similar to WT (Fig. 3*C*). The RKK mutants remained Ca^{2+} sensitive (*SI Appendix*, Fig. S6) and the RKK:VVV mutation increased P_o even when the C-terminal cytoplasmic domain was absent (*SI Appendix*, Fig. S7).

Mutations That Preserve Ion–Ion Interactions. The negative and positive charges are exchanged between positions 321/324 and 329–331 in E321R:E324R:R329E:K331E (EE-RKK:RR-EKE) and E321R:E324R:R329E:K330E:K331E (EE-RKK:RR-EEE); however, the ion–ion interactions should remain intact. Unlike the double mutation E321R:E324R (EE-RKK:RR-RKK) (blue solid curve in *SI Appendix*, Fig. S8), both EE-RKK:RR-EKE and EE-RKK:RR-EEE shifted $V_{0.5}$ to the positive direction (*SI Appendix*, Fig. S8, blue triangles and squares). Glu residues at positions 329–331 (the RKK segment) induced net destabilization of the open conformation, suggesting that the positive RKK segment in WT may have separate negative partners to stabilize the open conformation. Further, the voltage dependence of steady-state activation of EE-RKK:RR-EKE and EE-RKK:RR-EEE was very similar to that of EE-RKK:EE-EEE (*SI Appendix*, Fig. S8*B*, blue triangles and squares vs. red solid curve). The

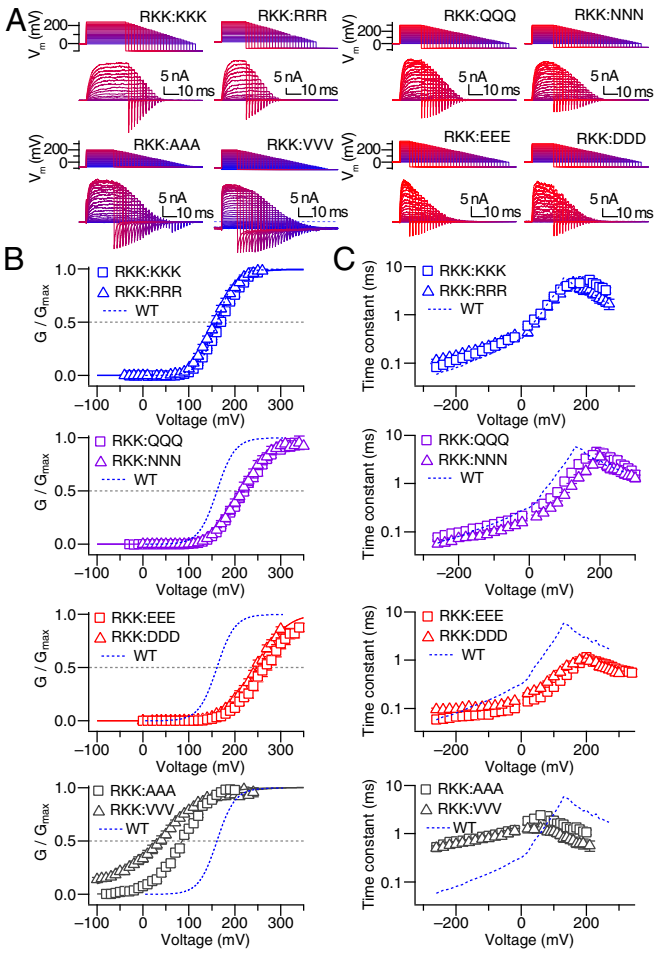

Fig. 3. Triple mutations of the RKK segment. (*A*) K^+ currents from R329K:K330K:K331K (RKK:KKK), R329R:K330R:K331R (RKK:RRR), R329Q:K330Q:K331Q (RKK:QQQ), R329N:K330N:K331N (RKK:NNN), R329A:K330A:K331A (RKK:AAA), R329V:K330V:K331V (RKK:VVV), R329E:K330E:K331E (RKK:EEE), and R329D:K330D:K331D (RKK:DDD). (*B*) Voltage dependence of current activation from the double mutants indicated. See *SI Appendix*, Table S1 for $V_{0.5}$ and Q_{app}. (*C*) Voltage dependence of current kinetics. The blue dashed curves represent WT. The results shown are means ± SD. Results were obtained with 0 Ca^{2+} with 11 mM EGTA.

presence of E321R and E324R in the R329E:K330E:K331E background made no difference in overall activation; the RKK segment must have a higher precedence as a gating determinant.

The voltage dependence of current kinetics of EE-RKK:RR-EKE and EE-RKK:RR-EEE at extreme positive and negative voltages was clearly shallower than that of WT, EE-RKK:RR-RKK, and EE-RKK:EE-EEE (*SI Appendix*, Fig. S8*C*). The deactivation voltage dependence at negative voltages of EE-RKK:RR-EEE was indistinguishable from that of EE-RKK:EE-EEE; the mutations E321R:E324R had no impact. Comparison of the deactivation kinetics of the EE-RKK:RR-EKE and EE-RKK:RR-EEE suggests that position 330 is an important determinant of the deactivation kinetics (*SI Appendix*, Fig. S8*C*).

Nonpolar Residues in the RKK Segment. We examined the functional properties of R329A:K330A:K331A (RKK:AAA), R329V:K330V:K331V (RKK:VVV), R329I:K330I:K331I (RKK:III), and R329L:K330L:K331L (RKK:LLL): substitutions of ^{329}RKK^{331} with nonpolar neutral amino acids. The mutations RKK:AAA and RKK:VVV shifted $V_{0.5}$ by −130 and −175 mV, respectively, and decreased Q_{app} (Fig. 3*B*, *Fourth Row*; *SI Appendix*, Table S2). These negative-going $V_{0.5}$ changes were accompanied by a striking slowing of current kinetics at negative voltages and shallower voltage dependence (Fig. 3*C*, *Fourth Row*). Substitutions of the RKK residues with nonpolar amino acids clearly stabilized the open conformation of the gate, and the stabilization was more readily observed in RKK:III and RKK:LLL (Fig. 4). Single-channel measurements showed that the P_o values of RKK:III and RKK:LLL at −240 mV without Ca^{2+} were about 0.2 and 0.4, respectively (Fig. 4 *A* and *B*), more than ∼100,000 times greater than that for WT (*SI Appendix*, Fig. S4). We roughly estimate their $V_{0.5}$ values to be about −158 mV and −217 mV (Fig. 4*B*), corresponding to shifts of −320 and −380 mV. At −240 mV, the mean burst open durations for the RKK:III and RKK:LLL mutants were ∼1 and 2 ms, respectively (Fig. 4*C*), ∼13–25 times greater than that for WT. Thus, most of the dramatic increase in P_o in RKK:III and RKK:LLL originated from their drastically shortened closed durations (Fig. 4*C*).

The RKK ring typically involved R329 and K331 but not K330 (Fig. 1*C*). We compared the properties of the double mutant R329E:K331E and the single mutant K330E (*SI Appendix*, Fig. S9, *Top Row*). In both voltage dependence of activation and current kinetics, K330E was similar to WT, while R329E:K331E with K330 intact closely resembled the triple mutant R329E:K330E:K331E; K330E had no measurable consequence.

The double mutant R329V:K331V with K330 remaining and the single mutant K330V with R329 and K331 intact were much more similar to WT than to RKK:VVV in voltage dependence of activation (*SI Appendix*, Fig. S9, *Bottom Row*). Even one positive residue compromised the open-state stabilization effect of the triple Val substitution; the collective hydrophobic characteristic must be crucial. We observed, however, that K330V alone slows down the deactivation kinetics at negative voltages without noticeably affecting the activation kinetics (*SI Appendix*, Fig. S9*C*, *Bottom Row*). In K330V, presumably, R329 and K331 may be forming the closed-state stabilizing interactions with E321/E324.

Fig. 4*D* plots the measured $V_{0.5}$ values of the triple RKK mutants according to the Wimley–White hydrophobicity scales (ΔG_{wif}) of the inserted amino acids (25). Among the neutral amino acids, a good linear relationship between $V_{0.5}$ and ΔG_{wif} is observed (Fig. 4*D*, gray-filled symbols). However, this relationship disappears when charged amino acids are included (Fig. 4*D*, red and blue symbols), suggesting that distinct physicochemical interactions are operative, depending on the amino acid type present.

Interactions That Stabilize the Open Conformation. The RKK segment appears to stabilize both the closed and open conformations of the ion conduction gate. To reveal the structural components stabilizing the open conformation, we inspected the simulated WT structures with Ca^{2+} and Mg^{2+} bound (Fig. 1). Additionally, we performed MD simulations of RKK:LLL without divalent cations. Both WT with Ca^{2+} and Mg^{2+} and RKK:LLL without divalent cations have high P_o values at 0 mV (>0.5 and >0.9, respectively); the gate is probably open. As already noted, the RKK segment contributes to the RKK ring in the divalent cation-free condition (Fig. 5 *A* and *B*, *Left*). With Ca^{2+} and Mg^{2+} bound, the RKK side chains are more likely to make ion–ion interactions with the O atoms of the phosphate and glycerol moieties of the membrane lipids (Fig. 5 *A* and *B*, *Center*). While R329 appears to make contacts with the lipid O atoms without divalent cations, K330 and K331 form more lipid O atom interactions when Ca^{2+} and Mg^{2+} are bound (Fig. 5*C*, red bars; *SI Appendix*, Figs. S10 and S11), presumably stabilizing the open conformation. If the RKK–lipid O atom interactions stabilize the open conformation, how do the hydrophobic substitutions such as RKK:LLL (Fig. 4) dramatically increase P_o? Our simulations of RKK:LLL show that the ^{329}LLL^{331} side chains interact with the hydrophobic tail groups of the lipids instead of the polar head groups (Fig. 5 *A* and *B*, *Right*). These hydrophobic interactions then stabilize the open conformation. In the hSlo1 RKK:LLL structures, the side chains of E321 and E324 are surrounded by water as in WT with Ca^{2+} and Mg^{2+} bound.

Comparison of the selectivity filter residues, ^{289}GYG^{291}, in the divalent cation-free structures ($P_o < 1 \times 10^{-4}$ at 0 mV), the Ca^{2+}- and Mg^{2+}-bound structures ($P_o > 0.5$ at 0 mV), and the RKK:LLL structures without divalent cations ($P_o > 0.9$ at 0 mV) reveals that the aforementioned filter residues in the latter two conditions are noticeably better organized to coordinate K^+ ions (Fig. 5*D* and Movie S1). In particular, the orderliness of ^{289}GYG^{291} in the RKK:LLL channel is striking. The channel pore status in the ^{289}GYG^{291} segment was evaluated with the software MOLE (26) (*SI Appendix*, Fig. S12). The pore radius estimates of RKK:LLL were appreciably larger than those with Ca^{2+} and

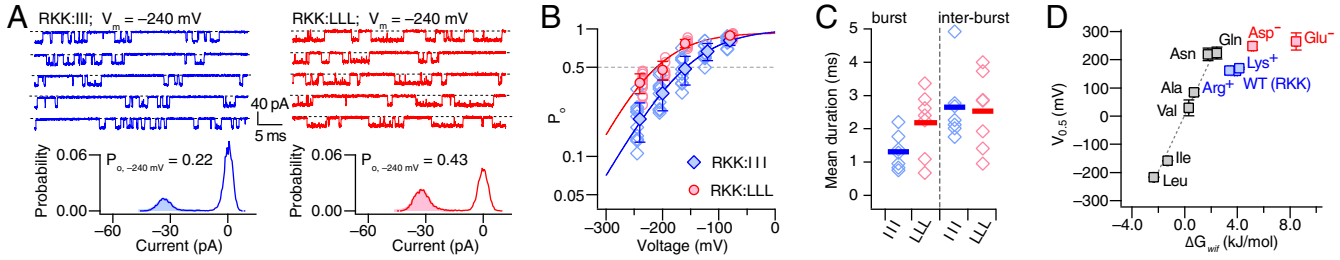

Fig. 4. RKK neutralization mutants are open at extreme negative voltages. (*A*) Openings at –240 mV from R329:I:K330I:K331I (RKK:III, *Top Left*) and R329L:K330L:K331L (RKK:LLL, *Top Right*). The dashed horizontal lines indicate the 0-pA level. Each patch contained one channel. All-points amplitude histograms are also shown (*Bottom*). (*B*) Voltage dependence of P_o for RKK:III and RKK:LLL ($n = 6$–13). The curves are Boltzmann-type fits (*SI Appendix*, Table S1). The data for RKK:III and RKK:LLL are shown with ±5 mV offsets for clarity. (*C*) Mean burst open and interburst closed durations for RKK:III and RKK:LLL at −240 mV. The thick horizontal bars indicate the mean values. (*D*) Relationship between $V_{0.5}$ and Wimley–White hydrophobicity (ΔG_{wif}) of the amino acid in the RKK segment in the mutants where each of the three ^{329}RKK^{331} residues is replaced with the amino acid indicated. The electrophysiological results are means ± SD. The Leu and Ile results were from single-channel measurements. Results were obtained with 0 Ca^{2+} with 11 mM EGTA.

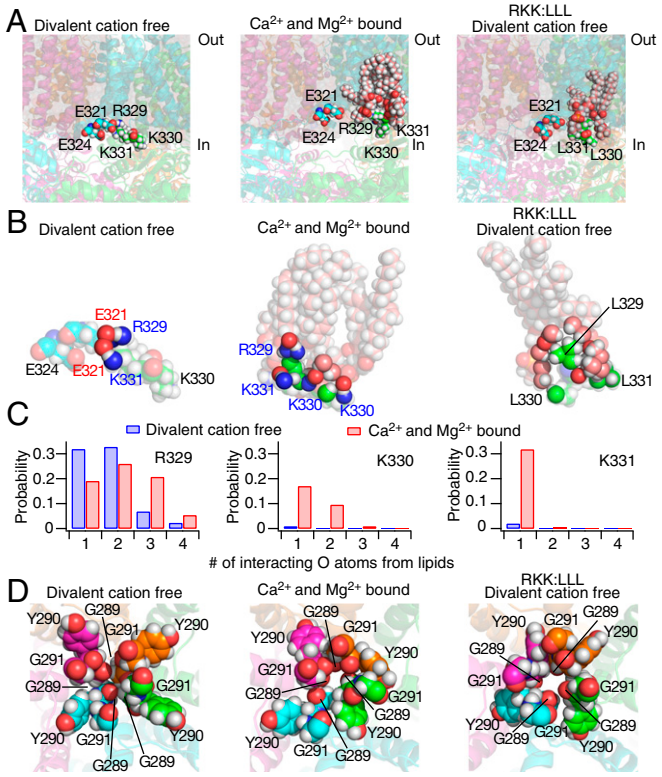

Fig. 5. Gating cycle-dependent interactions of the RKK segment with membrane lipids. (*A*) Snapshots of the simulation results from hSlo1 WT without divalent cations (*Left*), WT with Ca^{2+} and Mg^{2+} (*Center*), and RKK:LLL without divalent cations (*Right*). ^{329}RKK^{331}, E321, E324, the interacting lipid molecules, and pore K^+ ions are depicted using spheres. The ion conduction pathway runs in the center in the upper half of each image. (*B*) The RKK interaction partners under the three conditions indicated. Lipid carbon atoms are shown in pink. See *SI Appendix*, Fig. S10 for the remaining subunits. (*C*) Probability of the interactions between lipid O atoms and the residues indicated under the divalent cation-free condition (blue) and the Ca^{2+}- and Mg^{2+}-bound condition (red). The results are from an illustrative 100-ns run analyzed every 0.2 ns. (*D*) The selectivity filter residues viewed from the extracellular side. ^{289}GYG^{291} are shown using spheres. Ions, water, and lipid molecules are not shown. Similar results were obtained in all four simulation runs in each condition.

Mg^{2+} bound. Further, in the Ca^{2+}-free structures, a pore through the ^{289}GYG^{291} segment was often undetectable. The pore radius estimates of these structures are roughly proportional with the respective P_o values at 0 mV.

Discussion

Membrane phospholipids have been long regarded as an important contributor to ion channel gating. However, the exact mechanisms by which the lipids influence channel gating have been unclear. Our study on the sequence ^{329}RKK^{331} in hSlo1 at the C-terminal end of S6 near the protein–membrane interface provides a clear view of how the Slo1 channel interacts with nearby membrane lipids in a gating cycle-dependent way. Our results here lead to the following model whereby the ^{329}RKK^{331} segment influences WT Slo1 gating. When the ion conduction gate is closed, the side chains of R329 and K331 form ion–ion interactions with the side-chain O atoms of E321 and E324 in S6 of an adjacent subunit. This RKK-E321/E324 intersubunit ring stabilizes the closed conformation. When the gate is open, the RKK ring is broken. The RKK side chains are positioned away from the central pore axis and form electrostatic interactions with the nearby lipid O atoms, stabilizing the open conformation, while E321 and E324 interact with water. Therefore, for each closed–open gating cycle, the ^{329}RKK^{331} side chains alternate between the O atoms from E321/E324 and the membrane lipids. It may be noted that in the cyro-EM structure of solubilized and purified *Aplysia* Slo1 without divalent cations (5TJI) (20), the ^{329}RKK^{331} and E321/E324 equivalent residues do not form the interactions observed here in part because the side chains of the *Aplysia* residues equivalent to K330 and K331 are not resolved (20) (*SI Appendix*, *Materials and Methods*).

The above membrane phospholipid-dependent gating cycle model may be used to interpret the mutagenesis results described. Neutralization of E321 and/or E324 shifts the voltage dependence of activation to the negative direction, consistent with the idea that the closed conformation is destabilized because the ion–ion interactions forming the RKK ring are disrupted. Further, our single-channel measurements without Ca^{2+} at negative voltages show that the observed negative shifts in $V_{0.5}$ are probably attributable to changes in the intrinsic behavior of the ion conduction gate specified by the equilibrium constant L_0 in the HA model of Slo1 gating. Activation of the voltage sensors or that of the divalent cation sensors is not required, although our study does not directly assess their contributions. The mutational results covering ^{329}RKK^{331} are interpretable only if both the interactions affecting the closed conformation, ^{329}RKK^{331} and E321/E324, and those affecting the open conformation, ^{329}RKK^{331} and membrane lipids, are taken into account. The charge-preserving mutations RKK:KKK and RKK:RRR are largely without effect as expected. The charge-reversal mutations RKK:EEE and RKK:DDD break the RKK ring stabilizing the closed conformation but also fail to form the interactions with membrane lipid O atoms to stabilize the open conformation. Thus, their voltage dependence shifts to the positive direction. In both RKK:EEE and RKK:DDD, the side chains at positions 329–331 interact only with water regardless of the ion conduction gate status; the interactions with water do not appear effective because the activation and deactivation kinetics of RKK:EEE and RKK:DDD are much faster than WT. The charge-exchange mutations such as EE-RKK:RR-EEE preserve the RKK ring but Glu at positions 329–331 fail to interact with the lipid O atoms. The open state is destabilized and the voltage dependence shifts to the positive direction.

Substitutions of ^{329}RKK^{331} with hydrophobic amino acids, such as V, L, and I, remove the closed-state stabilizing positive charges. Additionally, neither V, L, nor I interact readily with the lipid O atoms to stabilize the open conformation. However, the side chains of V, L, and I form hydrophobic interactions with the tail groups of the nearby membrane lipids to stabilize the open conformation. Thus, in RKK:VVV, RKK:III, and RKK:LLL, the voltage dependence of activation shifts to the negative direction, the activation time course is faster (closed-state destabilization), and the deactivation time course is slower (open-state stabilization). The hydrophobic interactions between the channel and the lipid tails must be considerable; the shift in activation voltage dependence in RKK:LLL is nearly −400 mV. Using the single-channel P_o values of WT ($<2 \times 10^{-6}$) and RKK:LLL (~0.4) at −240 mV, the energy of the open-state stabilization by RKK:LLL is estimated to be ~30 kJ/mol/channel (12.1 k_BT/channel). Whether such a level of free energy could be attained by the structural differences involving the amino acids at positions 329–331 as suggested in the simulations (Fig. 5*B*) remains to be examined.

Some of the mutants examined showed shallower GV steepness as well as shallower voltage dependence of activation and deactivation kinetics. The HA model-based simulations (*SI Appendix*, Table S3) suggest that the shallower GV curves are caused by weakened coupling between the ion conduction gate and the primary voltage sensors: smaller D values in the HA model (13). The coupling process must depend on the positive charges at positions 329–331 because the GV steepness is unaltered in RKK:KKK and RKK:RRR. In addition, the voltage dependence of current activation kinetics at positive voltages reflecting opening of the ion conduction gate (δ_4 in the HA

model) and that of deactivation at negative voltages reflecting closing of the gate (γ_0 in the HA model) are also shallower in many mutants, for example, RKK:AAA and RKK:VVV. Multiple possible mechanisms exist. First, neutralization of the RKK segment may alter the local surface potential, which can modify the transmembrane electric profile. Second, the protein mutations may modify the structures of the surrounding membrane lipids and thus the transmembrane electric profile. Third, the altered voltage dependence may also be caused by changes in ion occupancy of the selectivity filter as suggested for the K_2P channel (27).

The MD simulation results show discernible differences in the selectivity filter region under the three conditions tested: WT without divalent cations, WT with Ca^{2+} and Mg^{2+} fully bound, and RKK:LLL without divalent cations. In the latter two conditions with very high P_o values at 0 mV, the selectivity filter residues (^{289}GYG^{291}) appear more organized to form a detectable pore. The same filter residues in the divalent cation-free condition with low P_o at 0 mV are less organized. These structural differences may be consistent with the suggestion that the selectivity filter is the primary ion conduction gate of Slo1 (4, 5). The filter distortion is also reminiscent of a C-type inactivated state of a Kv channel (28). It is remarkable that such structural changes at the ^{289}GYG^{291} filter region are visible as a consequence of divalent cation binding or mutations at the intracellular side. A similar structural distortion of the selectivity filter is absent in the cryo-EM structure of solubilized *Aplysia* Slo1 without divalent cations developed with symmetry constraint (20). Further, the filter distortion was not detected in a simulation study by Jia et al. (7). One contributing factor to the differing results of Jia et al. and this study may be the initial K^+ occupancy in the selectivity filter. The simulation systems in Jia et al. contained a K^+ ion in each of the K^+ sites (S0–S4) without any water, whereas our systems had K^+ ions in S0, S2, and S4, and water in S1 and S3.

The membrane phospholipid-dependent gating cycle model of Slo1 may be helpful in understanding how the channel gating is influenced by diverse amphipathic molecules such as PIP_2 (14–16), hemin (29), and omega-3 docosahexaenoic acid (30). One aspect of the PIP_2 action involves the RKK segment (14, 16), and intracellular PIP_2 may compete with E321 and E324 for ion–ion interactions with ^{329}RKK^{331}, destabilizing the closed conformation. If the long PIP_2 tail group is well incorporated into the membrane, the open conformation may stabilize through the embedded PIP_2–^{329}RKK^{331} interactions. This idea may explain why short, water-soluble PIP_2 analogs are less effective (14).

In summary, our study suggests that the closed state of the Slo1 channel is stabilized by intraprotein ion–ion interactions involving the RKK segment and that in the open state the RKK segment makes more intimate contacts with the membrane phospholipids. We suggest that the channel–lipid interactions are formed and broken each time the channel opens and closes. When the gate, whose physicochemical nature remains to be revealed, is open, the selectivity filter residues are well organized to pass K^+ ions. The importance of the membrane phospholipids in each gating cycle of the Slo1 channel may provide a framework to understand the mechanisms of actions of cell signaling molecules and pharmacological modulators of the channel.

Materials and Methods

Homology models of hSlo1 channels were made from *Aplysia* Slo1 channels (20, 21), and MD simulations were carried out with NAMD2 using the CHARMM36m force field. Electrophysiological measurements were performed under a symmetrical 140-mM K^+ condition using human embryonic kidney tsA 201 cells. Detailed materials and methods are found in *SI Appendix*.

ACKNOWLEDGMENTS. The study was supported in part through NIH Grant R01GM121375 (to T.H.) and German Research Foundation Grants FOR1738 and HE2993/18-1 (to S.H.H.).

1. Horrigan FT, Aldrich RW (2002) Coupling between voltage sensor activation, Ca^{2+} binding and channel opening in large conductance (BK) potassium channels. *J Gen Physiol* 120:267–305.
2. Hoshi T, Pantazis A, Olcese R (2013) Transduction of voltage and Ca^{2+} signals by Slo1 BK channels. *Physiology (Bethesda)* 28:172–189.
3. Pantazis A, Olcese R (2016) Biophysics of BK channel gating. *Int Rev Neurobiol* 128:1–49.
4. Wilkens CM, Aldrich RW (2006) State-independent block of BK channels by an intracellular quaternary ammonium. *J Gen Physiol* 128:347–364.
5. Yan J, Li Q, Aldrich RW (2016) Closed state-coupled C-type inactivation in BK channels. *Proc Natl Acad Sci USA* 113:6991–6996.
6. Schewe M, et al. (2019) A pharmacological master key mechanism that unlocks the selectivity filter gate in K^+ channels. *Science* 363:875–880.
7. Jia Z, Yazdani M, Zhang G, Cui J, Chen J (2018) Hydrophobic gating in BK channels. *Nat Commun* 9:3408.
8. Long SB, Tao X, Campbell EB, MacKinnon R (2007) Atomic structure of a voltage-dependent K^+ channel in a lipid membrane-like environment. *Nature* 450:376–382.
9. Chen X, Yan J, Aldrich RW (2014) BK channel opening involves side-chain reorientation of multiple deep-pore residues. *Proc Natl Acad Sci USA* 111:E79–E88.
10. Zhou Y, Xia XM, Lingle CJ (2011) Cysteine scanning and modification reveal major differences between BK channels and Kv channels in the inner pore region. *Proc Natl Acad Sci USA* 108:12161–12166.
11. Soom M, Gessner G, Heuer H, Hoshi T, Heinemann SH (2008) A mutually exclusive alternative exon of slo1 codes for a neuronal BK channel with altered function. *Channels (Austin)* 2:278–282.
12. Gonzalez-Perez V, Lingle CJ (2019) Regulation of BK channels by beta and gamma subunits. *Annu Rev Physiol* 81:113–137.
13. Hoshi T, Heinemann SH (2016) Modulation of BK channels by small endogenous molecules and pharmaceutical channel openers. *Int Rev Neurobiol* 128:193–237.
14. Vaithianathan T, et al. (2008) Direct regulation of BK channels by phosphatidylinositol 4,5-bisphosphate as a novel signaling pathway. *J Gen Physiol* 132:13–28.
15. Tang QY, Zhang Z, Meng XY, Cui M, Logothetis DE (2014) Structural determinants of phosphatidylinositol 4,5-bisphosphate (PIP2) regulation of BK channel activity through the RCK1 Ca^{2+} coordination site. *J Biol Chem* 289:18860–18872.
16. Tian Y, et al. (2015) Two distinct effects of PIP2 underlie auxiliary subunit-dependent modulation of Slo1 BK channels. *J Gen Physiol* 145:331–343.
17. Suh BC, Hille B (2008) PIP_2 is a necessary cofactor for ion channel function: How and why? *Annu Rev Biophys* 37:175–195.
18. Hansen SB, Tao X, MacKinnon R (2011) Structural basis of PIP_2 activation of the classical inward rectifier K^+ channel Kir2.2. *Nature* 477:495–498.
19. Gessner G, et al. (2012) Molecular mechanism of pharmacological activation of BK channels. *Proc Natl Acad Sci USA* 109:3552–3557.
20. Hite RK, Tao X, MacKinnon R (2017) Structural basis for gating the high-conductance Ca^{2+}-activated K^+ channel. *Nature* 541:52–57.
21. Tao X, Hite RK, MacKinnon R (2017) Cryo-EM structure of the open high-conductance Ca^{2+}-activated K^+ channel. *Nature* 541:46–51.
22. Zhang Y, Niu X, Brelidze TI, Magleby KL (2006) Ring of negative charge in BK channels facilitates block by intracellular Mg^{2+} and polyamines through electrostatics. *J Gen Physiol* 128:185–202.
23. Zhang G, et al. (2014) A charged residue in S4 regulates coupling among the activation gate, voltage, and Ca^{2+} sensors in BK channels. *J Neurosci* 34:12280–12288.
24. Horrigan FT, Cui J, Aldrich RW (1999) Allosteric voltage gating of potassium channels I. Mslo ionic currents in the absence of Ca^{2+}. *J Gen Physiol* 114:277–304.
25. Wimley WC, White SH (1996) Experimentally determined hydrophobicity scale for proteins at membrane interfaces. *Nat Struct Biol* 3:842–848.
26. Sehnal D, et al. (2013) MOLE 2.0: Advanced approach for analysis of biomacromolecular channels. *J Cheminform* 5:39.
27. Schewe M, et al. (2016) A non-canonical voltage-aensing mechanism controls gating in K2P K^+ channels. *Cell* 164:937–949.
28. Pau V, Zhou Y, Ramu Y, Xu Y, Lu Z (2017) Crystal structure of an inactivated mutant mammalian voltage-gated K^+ channel. *Nat Struct Mol Biol* 24:857–865.
29. Horrigan FT, Heinemann SH, Hoshi T (2005) Heme regulates allosteric activation of the Slo1 BK channel. *J Gen Physiol* 126:7–21.
30. Tian Y, et al. (2016) Atomic determinants of BK channel activation by polyunsaturated fatty acids. *Proc Natl Acad Sci USA* 113:13905–13910.